

Improved spatial filtering velocimetry and its application in granular flow measurement

Ping Kong(孔平), Bi-De Wang(王必得), Peng Wang(王蓬), Zivkovic V, Jian-Qing Zhang(张建青)

Citation: Chin. Phys. B . 2020, 29(7): 074201 . **doi:** 10.1088/1674-1056/ab8ac2
Journal homepage: http://cpb.iphy.ac.cn; http://iopscience.iop.org/cpb

What follows is a list of articles you may be interested in

Wide color gamut switchable autostereoscopic 3D display based on directional quantum-dot backlight

Bin Xu(徐斌), Xue-Ling Li(李雪玲), Yuan-Qing Wang(王元庆)

Chin. Phys. B . 2019, 28(12): 124208 . **doi:** 10.1088/1674-1056/ab53d1

Enhancement of spatial resolution of ghost imaging via localizing and thresholding

Yunlong Wang(王云龙), Yingnan Zhou(周英男), Shaoxiong Wang(王少雄), Feiran Wang(王斐然), Ruifeng Liu(刘瑞丰), Hong Gao(高宏), Pei Zhang(张沛), Fuli Li(李福利)

Chin. Phys. B . 2019, 28(4): 044202 . **doi:** 10.1088/1674-1056/28/4/044202

Sub-Rayleigh imaging via undersampling scanning based on sparsity constraints

Chang-Bin Xue(薛长斌), Xu-Ri Yao(姚旭日), Long-Zhen Li(李龙珍), Xue-Feng Liu(刘雪峰), Wen-Kai Yu(俞文凯), Xiao-Yong Guo(郭晓勇), Guang-Jie Zhai(翟光杰), Qing Zhao(赵清)

Chin. Phys. B . 2017, 26(2): 024203 . **doi:** 10.1088/1674-1056/26/2/024203

An improved transmitting multi-layer thin-film filter

Zhang Ying, Qi Hong-Ji, Yi Kui, Wang Yan-Zhi, Sui Zhan, Shao Jian-Da

Chin. Phys. B . 2015, 24(5): 054212 . **doi:** 10.1088/1674-1056/24/5/054212

A 23.75-GHz frequency comb with two low-finesse filtering cavities in series for high resolution spectroscopy

Hou Lei, Han Hai-Nian, Wang Wei, Zhang Long, Pang Li-Hui, Li De-Hua, Wei Zhi-Yi

Chin. Phys. B . 2015, 24(2): 024213 . **doi:** 10.1088/1674-1056/24/2/024213

Improved spatial filtering velocimetry and its application in granular flow measurement*

Ping Kong(孔平)[1], Bi-De Wang(王必得)[2], Peng Wang(王蓬)[3,1], Zivkovic V[4], and Jian-Qing Zhang(张建青)[5,†]

[1] *Shanghai Key Laboratory for Molecular Imaging, Shanghai University of Medicine and Health Sciences, Shanghai* 201318, *China*
[2] *School of Optical-Electrical and Computer Engineering, University of Shanghai for Science and Technology, Shanghai* 200093, *China*
[3] *School of Medical Instrument and Food Engineering, University of Shanghai for Science and Technology, Shanghai* 200093, *China*
[4] *School of Chemical Engineering and Advanced Materials, Newcastle University, NE*1 7*RU, United Kingdom*
[5] *College of Medical Imaging, Shanghai University of Medicine and Health Sciences, Shanghai* 201318, *China*

(Received 26 February 2020; revised manuscript received 17 March 2020; accepted manuscript online 18 April 2020)

Spatial filtering velocimetry (SFV) has the advantages of simple structure, good stability, and wide applications. However, the traditional linear CCD-based SFV method requires an accurate angle between the direction of linear CCD and the direction of moving object, so it is not suitable for measuring a complex flow field or two-dimensional speed in a granular media. In this paper, a new extension of spatial filtering method (SFM) based on high speed array CCD camera is proposed as simple and effective technique for measuring two-dimensional speed field of granular media. In particular, we analyzed the resolution and range of array CCD-based SFV so that the reader can clarify the application scene of this method. This method has a particular advantage for using orthogonal measurement to avoid the angle measurement, which were problematic when using linear CCD to measure the movement. Finally, the end-wall effects of the granular flow in rotating drum is studied with different experimental conditions by using this improved technique.

Keywords: spatial filtering velocimetry, array CCD, end-wall effects, resolution

PACS: 42.30.–d, 47.11.–j, 47.57.Gc **DOI:** 10.1088/1674-1056/ab8ac2

1. Introduction

Granular materials are ubiquitous in the nature and important in various industries. The granular material exhibits a peculiar flow behavior that it can show both flow characteristics of the solid and the liquid depending on the conditions.[1] Therefore, research on granular flow has been a hot and difficult topic in the past few decades. Among a number of physical quantities that can characterize the motion features of the granular flow, speed is the most essential feature for characterizing the motion of granular flow. In particle's speed measurement field, particle image velocimetry (PIV) and particle tracking velocimetry (PTV) are two of the most common used methods. They can measure both particle's speed[2–5] and acceleration.[6–8] However, PTV requires a clear image of each particle, which means this method needs more stringent experimental conditions and equipment. Although PIV does not need a clear image with each particle, in order to obtain large signal-to-noise ratio (SNR) images, the experimental system requires very uniform illumination which is difficult to realize since the imaging and lighting system with the observed particles and accompanying scene have a complex interaction.[9–14]

Spatial filtering velocimetry (SFV) is another method that can measure granular flow speed. Compared with the mentioned methods above, the main advantages of this method are high resolution, non-contact, and strong environmental adaptability. It does not require a clear image of each particle. In the scenes where it is not easy to obtain a high SNR image, this method will be more suitable than PIV due to non-uniform illumination and other factors.[15] In the 1960s, Ator[16] first proposed the concept of spatial filtering method (SFM) and applied it to the measurement of the movement of particle motion in the air. Since then this method was used to measure the speed of rough surface fluid and solid–liquid two-phase flows.[17–20] With time and development of new spatial filtering methods, CCD cameras have gradually replaced traditional structural gratings. The CCD camera acts as a spatial filter and a photo-receiving device, making the speed measurement structure much simpler. Uddin *et al.*[21] used a linear CCD to simulate a traditional grating in a spatial filter system for the first time. Yang *et al.*[22,23] used a linear CCD to measure the speed of irregular particles in the rotating drum and showed that the method is suitable for granular flow measurements. One drawback of the linear CCD-based SFV for granular flow applications is the need to accurately measure the angle between the pixel array and the direction of motion in actual measurement, which limits granular flow applications

*Project supported by the National Natural Science Foundation of China (Grant No. 11902190), the Construction Project of Shanghai Key Laboratory of Molecular Imaging (Grant No. 18DZ2260400), and the Fund from the Shanghai Municipal Education Commission, China (Class II Plateau Disciplinary Construction Program of Medical Technology of SUMHS, 2018-2020).

†Corresponding author. E-mail: zhangjq@sumhs.edu.cn

© 2020 Chinese Physical Society and IOP Publishing Ltd

as usually the angle cannot be accurately determined. On the other hand, granular flow is almost never one-dimensional as accessible by linear-based SFV so a strong need is to extend the technique to measure two-dimensional speed.

In recent years, with the emergence of more and more complex scenes, researchers proposed a new SFV method based on array CCD camera.[24] This is a great improvement in the field of SFV at the time. Array CCD-based SFV can measure the speed components in orthogonal direction, so the errors caused by angular measurement can be avoided. Therefore, array CCD can replace linear CCD as the main device of spatial filtering system especially in the context of granular material flow measurement. However, as far as we know, there is no detailed study about parameters such as system' resolution and range, *etc*.

On the basis of the above description, this paper makes a further study on the array CCD-based SFV, especially study the sensitivity, range, and temporal-spatial resolution of the measurement system. In this measurement, we focused on the end-wall effects of granular flow in rotating drum[25] as important phenomena to be studied, since the previous paper[26] did not study the continuous state of the granular flow. Finally, the influences of different factors on the end-wall effects are presented and discussed.

2. Principle and setup

2.1. Principle of traditional SFV

Spatial filter velocimetry is used to measure the speed by observing the optical image of the moving object through a set of parallel slits or transmission gratings. Figures 1(a) is a schematic illustration of SFV measurement system. The entire system consists of light source, objective lens, spatial filter device, focusing lens, and photodetector. The light source is irradiated on a surface moving with a speed v, and the light is scattered from the moving surface. The scattered light is imaged by the objective lens on a spatial filter composed of a grating, the light passing through the grating is focused by the focusing lens and then received by the photodetector. Due to the narrow bandpass filtering characteristics of the spatial slit, the photodetector outputs a periodically varying sinusoidal signal containing the speed information. Figure 1(b) shows the generation process of the periodic signal. Since the object to be measured has a sustained speed v and the grating has a spatial period length p (interval between the grating parallel slits), the output signal of the photodetector has a stable period $T_0 = p/v_0$ where v_0 is the speed of the scattered image which is proportional to v in M. According to the relationship $f_0 = 1/T_0$ between period and frequency, the speed of moving objects can be calculated using the following equation:[27]

$$v = \frac{p \cdot f_0}{M \cdot \cos\theta}, \tag{1}$$

where M is the magnification of optical system, and θ is the angle between pixel array and speed direction.

Due to the complexity of structures, the difficulty of processing, and the fixed space period, the traditional SFV system with transmission grating and thermoelectric sensor structure has been gradually replaced by CCD/CMOS cameras. The use of CCD cameras greatly simplifies the system structure, and increases flexibility and stability. The traditional linear CCD which replaced the traditional grating in the early stage cannot meet the requirement of measurement for multi-directional speed, so the array CCD has become the main acquisition device in current SFV system[28,29] to study the end-wall effects in our simple rotating drum.

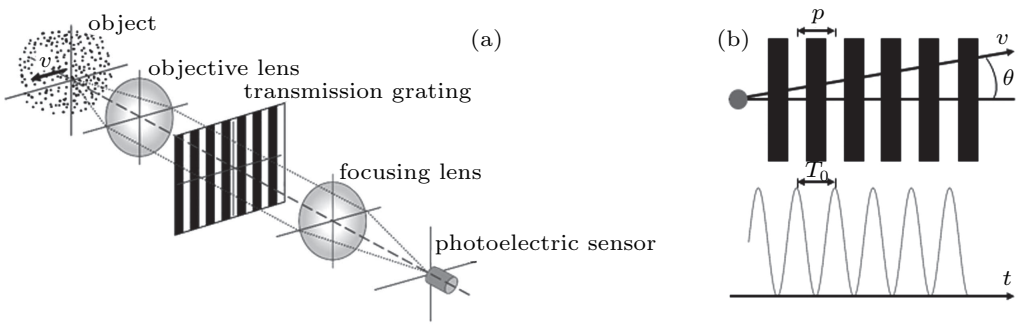


Fig. 1. Schematic diagram of (a) SFV measurement system and (b) spatial filtering signal generation process.

2.2. Spatial filtering effect

According to the analysis above, the most important problem of the spatial filtering velocimetry system is the spatial filtering effect produced by the grating. Let $f(x,y)$ be the light intensity distribution and $h(x,y)$ be the light intensity transmittance. Supposing the image moves with speed components v_x and v_y in directions x and y, respectively. The signal obtained by the photodetector can be expressed by the following formula:[30]

$$g(x_r, y_r) = \iint f(x_r - x, y_r - y)\, h(x,y)\mathrm{d}x\mathrm{d}y, \tag{2}$$

where $x_r = v_x t + c_1$, $y_r = v_y t + c_2$. In general, $f(x,y)$ is considered to satisfy the random traversal process. So, the auto-

correlation function of the output signal is

$$R(\tau_x, \tau_y) = E[g(x_r + \tau_x, y_r + \tau_y)\, g^*(x_r, y_r)], \tag{3}$$

where $E[X]$ means the expectation operation.[31] Perform Fourier transform on Eq. (3), we can get the power spectral density function

$$G_{\mathrm{P}}(\mu, \gamma) = F_{\mathrm{P}}(\mu, \gamma) H_{\mathrm{P}}(\mu, \gamma), \tag{4}$$

where $F_{\mathrm{P}}(\mu, \gamma)$ and $H_{\mathrm{P}}(\mu, \gamma)$ represent power spectral density functions of $f(x,y)$ and $h(x,y)$, respectively. In order to simplify the following expression, we assume that the object moves at speed v along x direction. Integrate Eq. (4), we can finally obtain the power spectral density function $G_{\mathrm{P}}(f)$ in the time domain

$$G_{\mathrm{P}}(f) = \frac{1}{v} \int_{-\infty}^{\infty} F_{\mathrm{P}}(f/v, \gamma) H_{\mathrm{P}}(f/v, \gamma) \mathrm{d}\gamma, \tag{5}$$

where $\mu = f/v$. The function $G_{\mathrm{P}}(f)$ will contain a peak frequency that can be used to calculate the speed of the object.

2.3. Principle of array CCD-based SFV

Array CCD is a photodetector composed of discrete pixels. By selecting a specific pixel unit, the traditional grating can be simulated by the array CCD as a spatial filter for measurement. The schematic diagram of the array CCD simulating the spatial filter in the horizontal direction is shown in Fig. 2. Supposing there are X_n pixels in the horizontal direction and Y_n pixels in the vertical direction, the horizontal speed of the particle motion is V_x, and the speed in the vertical direction is V_y. Taking the horizontal direction X as an example, the area to be tested on the image of the i frame is selected, all the pixels in this region can be divided into odd-numbered columns and even-numbered columns, which are structurally equivalent to two spatial filters whose phases are different by half a period. The X_n pixel values of each column are added, and the sum $B_{2,i}$ of the even columns is subtracted from the sum $B_{1,i}$ of all the odd columns to obtain differential output A of the analog filter of single image. Repeat the above steps for all frame images, a sample sequence $A = (A_1, A_2, \ldots, A_i, \ldots, A_n)$ can be obtained, where n is the number of frames of the acquired image. The sequence A is embodied in the time domain as a periodic sinusoidal function. Performing Fourier transform on the sequence to get the spectrum function, then correcting the spectrum function with the energy barycenter correction[32] so that we can determine the peak frequency f_0 accurately, and finally we calculate the horizontal speed V_x by f_0. More details of the above correction method can be found in our recent paper.[33]

Each of the light-transmitting area and the light-shielding area constitutes a spatial period P, which is represented as an adjacent odd-numbered column and an even-numbered column on the image, and the number of spatial periods n can be obtained by dividing the total number of columns by the space period P. Speed V_y in the vertical direction of the object can be obtained in the same way. Finally, the actual moving speed, V, of the object can be calculated according to the vector summation formula.

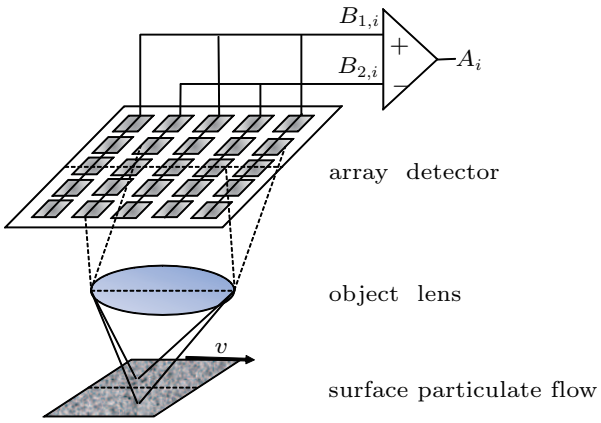


Fig. 2. Principle of array CCD-based SFV.

2.4. Experimental setup

According to the array CCD-based SFV principle and the actual measurement demand, the drum granular flow speed measuring system is constructed, as shown in Fig. 3(a). The experimental device is composed of white light source, array CCD camera, rotating drum device, and turntable. Fixing the lens-mounted array CCD on the bracket and adjust the shooting angle so that the lens is parallel to the surface of the granular flow. The light source in the system is a white LED light, and the array CCD what we used is a QianYanLang 3F04M high-speed camera with 2320×1720 pixels and a single pixel size of 7.7 μm. The lens is a fixed-focus lens designed by NIKON, and the focal length is 35 mm. The rotating drum with the particles is placed on the horizontal turntable, and the array CCD continuously photographs the surface of the granular flow, the images are stored to a computer for off-line analysis.

The rotating drums used in this article are all made of plexiglass and driven by a DC motor on a turntable. The diameter of the drum is 140 mm with 3 different drum lengths of 100 mm, 150 mm, 200 mm. The particles are all glass beads with a density of 2.7 g/cm^3, and the selected sizes are 0.5 mm, 1 mm, and 2 mm. A sample of 1-mm diameter glass beads is shown in Fig. 3(b).

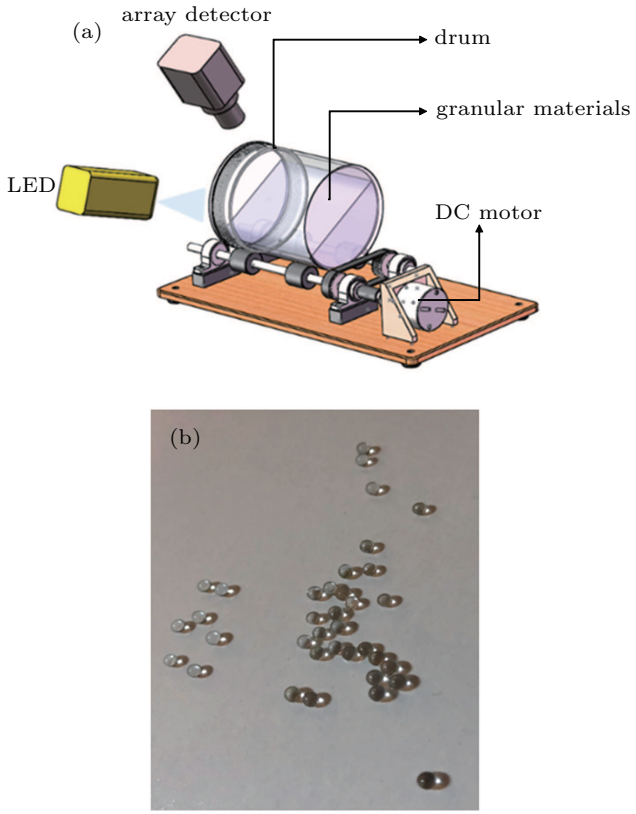


Fig. 3. (a) Schematics of array CCD-based SFV measurement system applied to rotating drum. (b) Sample picture of 1-mm diameter glass beads.

3. System parameter

3.1. Accuracy

In order to verify the effectiveness of the measurement system and evaluate the accuracy of the array CCD measurement system, first, the SFV measurement system was used to measure a uniform moving conveyor belt. Figure 4(a) shows schematics of the measuring conveyor speed system. Fixing the array CCD and the lens on a bracket, adjusting the shooting angle to make sure that the pixel plane is parallel to the belt motion plane, then we select the appropriate shooting height and focal length to obtain the measurement image of the belt. Figure 4(b) shows an example of the original movie frame of the conveyor belt from the movie recorded at a frame rate of 1000 Hz.

After setting up the measuring system, the amplification M, which can be calculated according to the ratio of the actual length of the object to the number of pixels it occupies in the picture, should be determined first. The belt width is 10^4 μm, and the number of pixels (single pixel width is 7 μm) the belt occupies in the picture is 81, so the system amplification factor can be calculated as 0.0567. Measurement of granular flow does not require changing the device position and system parameters, so the magnification in the following experiment is the same. In order to verify that the array CCD-based SFV will not be affected by the placement angle, first we adjust the angle between the conveyor belt and the array CCD, and take the images at different angles for speed measurement; to verify the rationality of multi-point measurement scheme for segmentation of array CCD into multiple sub-filters, two regions S1 and S2 are selected from the original image as sub-filters for speed measurement.

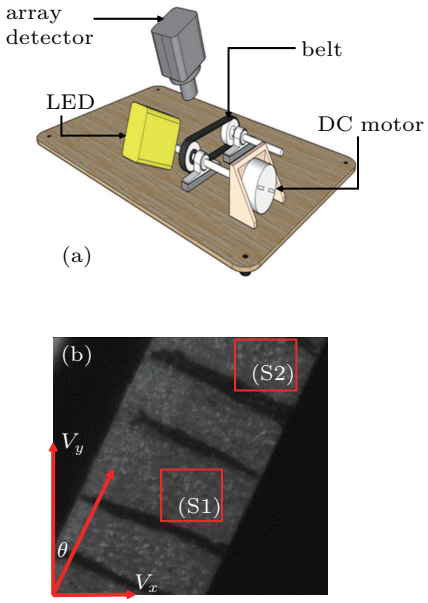


Fig. 4. (a) Conveyor belt speed measurement system. (b) Example of original image collected by the array CCD used in analysis with two regions of interest (S1 and S2) outlined.

The experiment set the conveyor speed V from 3 cm/s to 9 cm/s in 3-cm/s step value for a total of three speed values, besides, we set two different angles 30° and 45° for measurement. All of the following data are the average of ten experimental runs. Table 1 is the comparison data of the speeds calculated from the two different angles 30° and 45° in S1 area. It can be seen that the two sets of data are basically consistent with the actual values. Table 2 compares the measurement results of the central and edge regions of the CCD at 30°. According to the measurement data, it is obvious that the measurement speed of the two regions are consistent. The relative experimental error calculated as $(V_\alpha - V)/V$ where V_α is actual measurement speed and V is theoretical speed are also given in the table.

Table 1. Multi-angle speed comparison results in region S1.

V/(cm/s)	V_{30}/(cm/s)	Error/%	Std	V_{45}/(cm/s)	Error/%	Std
3	3.019	0.6	0.029	3.009	0.3	0.016
6	6.096	1.6	0.02	6.062	1	0.062
9	9.117	1.3	0.034	9.174	1.9	0.027

Table 2. Multi-point measurement results for 30° angle between conveyor belt and array CCD.

V/(cm/s)	V_{S1}/(cm/s)	Error/%	Std	V_{S2}/(cm/s)	Error/%	Std
3	3.019	0.6	0.029	3.016	0.5	0.032
6	6.096	1.6	0.02	5.925	1.3	0.015
9	9.117	1.3	0.034	8.917	0.9	0.03

Comparing the above data, it can be found that the array CCD-based SFV method is not affected by the placement angle, and the maximum error is less than 1.9%, which is lower than the linear CCD-based SFV method proposed by our team before (the maximum error is 2.46%).[22] Compared with the speeds in S1 and S2 regions, it can be found that the speed calculation results between the two regions are consistent. Array CCD can perform multi-point measurement on granular flow speed field which makes up for the deficiency of the linear CCD. Therefore, spatial filtering velocimetry measurement based on array CCD is feasible and superior to spatial filtering velocimetry measurement based on linear CCD.

3.2. Range

If the object to be tested moves at a constant speed v and the camera frame rate is r, then the distance that the object actually moves during the time interval t between two adjacent frames is

$$L = v \cdot t = v \cdot \frac{1}{r}. \tag{6}$$

For an installed speed measuring system, the magnification is constant, assuming the magnification is M, and the length of the moving object reflected in the CCD camera is l, according to the proportional relationship between the object and the image $M = l/L$, the following expression can be obtained:

$$v = \frac{l}{M} \cdot r. \tag{7}$$

It can be seen from Eq. (7) that when the speed measuring system is installed, the actual measured speed range is only related to the camera frame rate

$$\frac{l}{M} \cdot r_{\min} < v < \frac{l}{M} \cdot r_{\max}, \tag{8}$$

where $r_{\min}$ is the minimum frame rate while $r_{\max}$ is the maximum frame rate

3.3. Resolution

The system resolution includes time resolution R_t and a spatial resolution R_s. Theoretically, R_t and R_s are only related to the CCD camera characteristics. The time resolution $R_t = 1/f$ is determined by the camera frame rate f. Increasing the frame rate f, the time interval between the two frames becomes shorter and the continuity of the output signal gets better, then the surface speed of the granular flow will be more accurate. The maximum frame rate of the camera used in this experiment is 40600 frames per seconds (fps), so the minimum time resolution R_{tmin} is 1/40600 s. The spatial resolution $R_s = n \cdot p$ is determined by the space period size p and the slit number n. Generally, at least two rows (columns) of pixels can form a spatial period. In order to obtain the speed information of the object to be tested, one spatial period is required at least. Therefore, the minimum spatial resolution of the system is the pixel width of the two rows (columns) of the CCD camera. The single pixel size of the CCD camera used in this experiment is 7 μm, considering the magnification of the experimental system, M, the minimum spatial resolution of the system is $R_{\text{smin}} = 14 \cdot M$ in units of μm.

In the actual situation, considering the real-time demands of the measurement and the granular flow setup, we need to choose the optimal R_t and R_s. After measuring and comparing the same motion scene with different frame rates, it can be found that when the camera frame rate set at 1000 fps, the signal will possess a large signal to noise ratio (SNR) enabling confident determination the peak frequency f_0. The increase of frame rate will lead to decrease in SNR introducing ambiguity in peak frequency determination which limits a real-time measurement. Therefore, the best time resolution is 0.001 s; when changing the space period to calculate the scene to be measured, we find that the output signal has the best periodicity when the space period is set to 100 μm–120 μm. When the spatial period p is constant, we will get a larger sensitive area when the analog slit number becomes large. The size of the sensitive area directly affects the filtering effect of the spatial filter, mainly in the amplitude and main peak bandwidth of the spatially filtered signal: the more the number of stripes is, the narrower the bandwidth of the main peak of the signal and the higher the resolution become. However, as n increases, the single measurement area gets larger, the measurable points in the whole area are reduced, the measurement accuracy is lowered. For the same position of the drum, we set the same space period size p and the different number of slits n. After multiple measurements and analysis, it can be found that the most suitable number of slits n is 10. Thus, the best spatial resolution is 1 mm.

4. Results and discussion

4.1. Speed distribution of granular flow in rotating drum

Figure 5 shows the typical speed distribution of the granular flow in the rolling state[33] using the developed technique described above. As shown in Fig. 5(a), the granular flow near the end-wall region creates trajectories that are bended toward the center of the drum. The frictional force of the end wall of the drum has a great influence on particles. Figure 5(b) is the normalized speed field distribution of the active granular flow layer. In order to investigate the axial speed distribution of the granular flow surface, each axial value has been normalized with the the peak axial speed $v_{\max}$. The measurement results are of the same order as our previous linear CCD-based SFV method measurements[22] and the observed phenomena are consistent with the results measured by Santomaso.[25] Observing the speed distribution of the granular flow, it can be

found that the axial speed distribution is not uniform. The granular flow speed near the end wall region is significantly smaller than the speed away from the end-wall region, and the peak speed of the axial region does not appear in the center of the drum, but appears in halfway between side-walls and center of the drum.

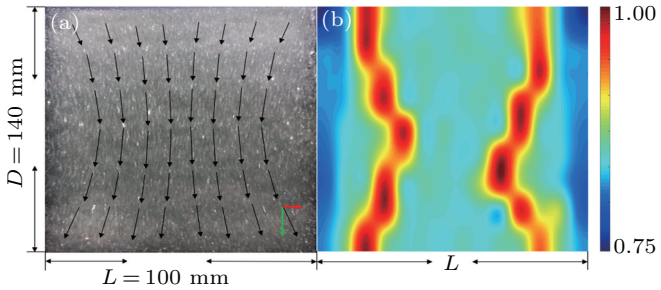


Fig. 5. (a) Trajectories of granular flow in the drum, arrows indicate the granular flow trajectory. Green and red arrows represent the vertical and axial speed, respectively, and black arrow represents the combined speed. (b) Normalized distribution of speed information of the granular flow. The drum is 100-mm long with 4-rpm speed and 40% filling degree, the particle size is 1 mm.

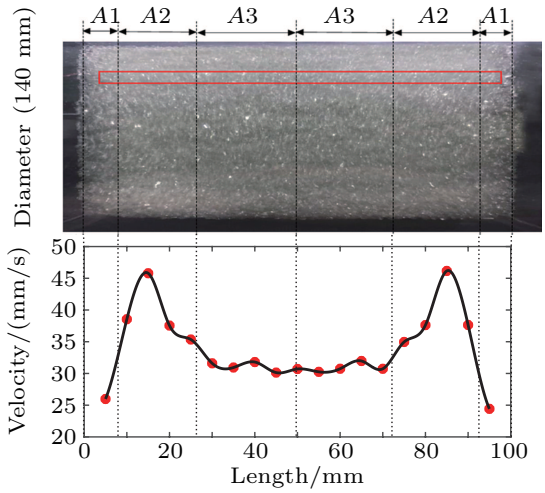


Fig. 6. (a) Raw image of the flowing layer of the drum showing red rectangular region of interest used for detailed analysis. (b) Speed distribution of granular flow for the red region. The particle size is 1 mm, and the drum rate is 3.7 rpm.

In order to study the axial flow variation of the drum particle, as shown in Fig. 6, the red rectangular region was selected to measure and analyze the speed profile in detail. The chosen rectangular region of the granular flow surface is divided into three pairs of axial sub-parts according to different speed profile characteristics. The granular flow speed in the end-wall region of the drum is smaller than the speed of particles away from the end-wall region. The reason is that the friction caused by the end wall cause particles in the region to slow down, and the particles away from the region are not affected by the friction force, the speeds are higher than those near the end wall. These near end-wall areas are set to be $A1$. A peak speed $v_{\max}$ appears in a region half-way from the end wall of the drum, this is because the frictional force on the end wall of the drum causes the granular flow speed lower than granular flow far from the end wall. According to the conservation of mass,[34] the granular flow near the end wall will compensate for the faster particles flowing away from the end wall. The flow of particles near the end wall will generate an axial force which will cause the flow to move obliquely in the center of the drum, the additional speed will superimpose the original speed of the granular flow, resulting in the appearance of the peak speed $v_{\max}$. The areas where the peak speed located are set to be $A2$. The axial speed will tend to be flatter away from the end wall, where the speed value is between the speed near the end wall and the peak speed, these areas are set to be $A3$.

The following part will specifically study the end-wall effects with different conditions. From the above speed distribution, it can also be found that the axial granular flow speed has symmetry in the axial direction, so all of the following results only show the speed distribution from the left side to the center axis of the drum. It should be noted that all the following works are carried out in the rolling state, since the end-wall effects in this state are more obvious.

4.2. End-wall effects with different parameters

4.2.1. Size factor

In order to investigate the influence of different drum lengths and particle sizes on the end-wall effects, we used different length drums and different size particles in experiments. Figure 7(a) shows the speed comparison of different lengths of the drum in the axial region. It can be seen that no matter how the drum length changed, the peak speed $v_{\max}$ of the $A2$ region appears at 15 mm–17 mm from the end wall. Therefore, the position of maximum speed, $L_{v\max}$, does not change with overall drum length. In addition, observing the $A3$ region, it can be found that the drum with the smaller length will lead to a higher speed in the $A3$ region. The difference is due to the fact that when the drum is narrower, the granular flow in $A1$ region will not only influence that in $A2$ region, owing to that $A1$ region is also close to $A3$ region, the granular flow in $A1$ region will also influence that in $A3$ region, so the speed of granular flow in $A3$ region is increased. The results are consistent with the surface flow in chutes of varying width (the streamwise speed increases as the width between the walls decreases).[35]

Figure 7(b) is a speed comparison in the axial region for different particle sizes. Similar to the results of changing the length of the drum, the change of particle size did not change the position of peak speed $L_{v\max}$ in $A2$, and the position of peak speed still appeared at the distance of 15 mm–17 mm from the end wall. In addition, the peak speed in $A2$ region and the speed in $A3$ stable region can also be changed by changing the particle size, when the particle sizes is 2 mm, the speed is only 2/3 of the corresponding position when the particle size is 0.5 mm.

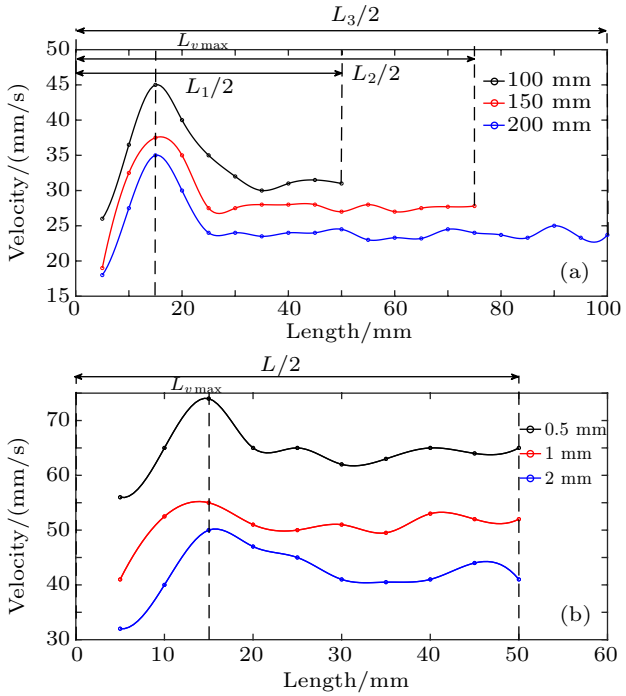


Fig. 7. (a) Axial speed distribution of 1-mm particles flow in different length cylinders at 2.5 rpm. (b) Axial speed distribution of particles flow for different particle sizes at 3.7 rpm. The particle filling degree is 40%, and the measurement area was set at 40 mm from upper end of the granular flow.

4.2.2. Drum speed

In this section the drum rotating speed is varied to study the effects of speed on the end-wall effects. As shown in Fig. 8, regardless of the drum rotation speed, the granular flow speed in the A1 region is still smaller than the granular flow speed in $A2$ and $A3$ regions, and the frictional force of the drum end wall still affects the granular flow movement near the end wall. When the drum speed is 2.5 rpm, the speed drops slowest from $A2$ region to $A3$ region, and the speed begins to stabilize at 30 mm from the end wall. In other word, the $A2$ region is increasing with the increase in rotational speed. In addition, it can be found that the effect of the end-wall effects on the peak speed $v_{\max}$ gradually decreases as the rotational speed increases, at the rotational speed of 4.5 rpm, the value of $v_{\max}$ compared to the speed in $A3$ region has become less prominent. Muzzio *et al.*[36] did similar experiments at larger drum speeds, combining with their measurements, we speculate that as the rotation speed of the drum increases, the influence of the inertial force on the granular flow is greater than the friction of the end wall, so when the speed superposition occurs in the peak speed region, the influence of the end-wall effects is not as prominent. In this case, the peak speed is closer in value to the speed in $A3$ region.

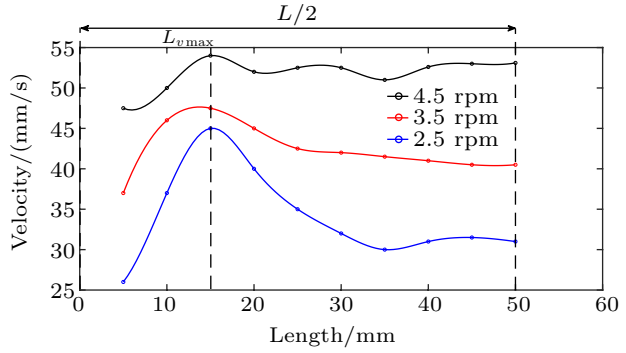


Fig. 8. Axial position speed distribution at different rotating speed drum. The particle filling degree is 40% while the particle size is 1 mm, and the length of drum is 100 mm. The measurement area is set at 40 mm from upper end of the granular flow.

4.2.3. Filling degree

Considering the degree of filling, since the surface area of the flow layer in different filling degrees is different in the same drum, the best solution is to compare the central axial area of the surface of the particle stream. Experimentally, when the filling degree is too low, the obtained motion fluctuates greatly, so the filling degree was changed from 30% to 50%.

As shown in Fig. 9, in the continuous flow state, changing the particle filling degree in the drum can significantly change the peak speed position, and as the filling degree is larger, the axial peak speed of the granular flow is closer to the central region. This is because when the degree of filling becomes larger, the contact area of the flow layer $A1$ region and the end wall of the drum increases,[37] so the flow of particles in the $A1$ region is subjected to greater frictional force, thereby generating a larger axial speed. The superposition of axial speed and vertical speed causes the peak axial speed to shift to the central area of the drum.

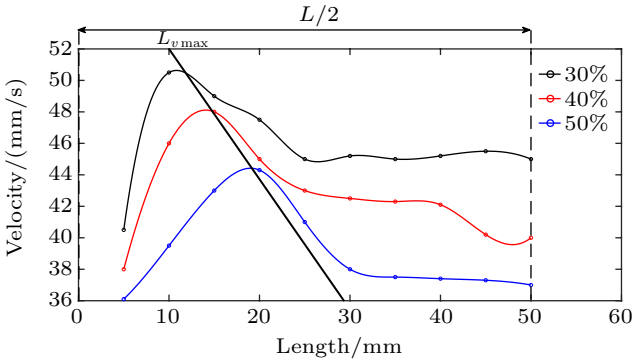


Fig. 9. The axial speed distribution for different filling degrees at 3.5 rpm. The experimental was performed with 1-mm particles in the 100-mm wide drum.

5. Conclusion

In the study of the speed field of particles surface flow within rotating drum, the end-wall effects cannot be ignored. We combined the SFV method with an array CCD and proposed an improved method for granular flow measurement. This paper focused on the SFV system's sensitivity, range, and temporal-spatial resolution. Compared with linear CCD, array CCD can not only obtain the entire surface flow field of the

particles but also eliminate the angular error by vector summation. Therefore, this method can accurately measure the whole field speed profile of the drum, so the end-wall effects of the rotating drum flow can be analyzed. By analyzing different drum parameters separately, this article also achieved got the following conclusions:

(i) End-wall effects of the drum occurs only in the end-wall regions at both ends, due to the friction of the end wall. The speed of the particles near the end wall is smaller than that of the particles away from the end wall. According to the law of conservation of momentum, a slow granular flow will compensate for the granular flow with a fast speed, which will result in an axial speed of the flow of particles. In addition, due to the effect of speed superposition, a peak speed occurs a little further from the end wall.

(ii) To reduce the influence of end-wall effects, the method of increasing drum rotating speed and length can be adopted. When the drum at a high rotating speed, the peak speed becomes less obvious and the end-wall effects area is shrinking. The main reason is that when the rotating speed of the drum increases, the influence of the inertial force on the granular flow caused by the drum rotation will be much greater than that of the friction force caused by the end wall. Although changing the length of the drum and the particle size does not affect the position of the peak speed, as the drum gets longer, the steady speed area in the middle of the drum will get larger, therefore, more effective values can be obtained in one experiment.

References

[1] Jaeger H M and Nagel S R 1992 *Science* **255** 1523
[2] Oudheusden V W B 2013 *Meas. Sci. Technol.* **24** 032001
[3] Chung Y C, Hsiau S S, Liao H H and Ooi J Y 2010 *Powder Technol.* **202** 151
[4] Song J, Yang H, Li R, Chen Q, Zhang Y J, Wang Y J and Kong P 2019 *Powder Technol.* **355** 172
[5] Wang B D, Song J, Li R, Han R, Zheng G and Yang H 2020 *Chin. Phys. B* **29** 014207
[6] Jensen A and Pedersen G K 2004 *Meas. Sci. Technol.* **15** 2275
[7] Ferrari S and Rossi L 2008 *Exp. Fluids* **44** 873
[8] Qiang Z D, Wang B D, Li R, Chen Q, Zheng G, Zivkovic V and Yang H 2020 *Powder Technol.* **360** 1037
[9] Stanier S, Dijkstrab J, Leśniewskac D, Hambletond J, Whitea D and Woodeba D M 2016 *Comput. Geotech.* **72** 100
[10] Yang H, Zhang B F, Li R, Zheng G and Zivkovic V 2017 *Powder Technol.* **311** 439
[11] Mou S H, Yang H, Li R, Zhang G H, Sun Q C and Kong P 2019 *Powder Technol.* **344** 1
[12] Yang H, Zhu Y H, Li R and Sun Q C 2020 *Particuology* **48** 160
[13] Zhang Y J, Yang H, Li R, Chen Q, Sun Q C and Kong P 2019 *Powder Technol.* **355** 333
[14] Zhu Y H, Yang H, Li R, Zhang Y J, Chen Q, Hua Y S, Sun Q C and Kong P 2020 *Powder Technol.* **360** 882
[15] Aizu Y and Asakura T 1987 *Appl. Phys. B* **43** 209
[16] Ator J T 1963 *J. Opt. Soc. Am.* **53** 1416
[17] Jakobsen M L and Hanson S G 2004 *Appl. Opt.* **43** 4643
[18] Burggraevea A, Hellings M, Remon J P, Vervaet C and Beer T D 2011 *Eur. J. Pharm. Sci.* **42** 584
[19] Xu C L, Li J and Wang S M 2012 *Flow Meas. Instrum.* **26** 68
[20] Han R, Zhang Y F, Li R, Chen Q, Feng J Y and Kong P 2020 *Chin. Phys. B* **29** 024501
[21] Uddin M S, Inaba H, Itakura Y and Kasahara M 1998 *Appl. Opt.* **37** 6234
[22] Gong J M, Yang H, Lin S H, Li R and Zivkovic V 2018 *Powder Technol.* **324** 76
[23] Lin S H, Yang H , Li R, Zheng G and Zivkovic V 2018 *Powder Technol.* **338** 376
[24] Schaeper M, Menn I, Frank H and Damaschke N 2008 14*th Int. Symp. on Applications of Laser Techniques to Fluid Mechanics* (Portugal: Lisbon) p. 1
[25] Santomaso A, Olivi M and Canu P 2004 *Chem. Eng. Sci.* **59** 3269
[26] Pohlman N A, Ottino J M and Lueptow R M 2006 *Phys. Rev. E* **74** 031305
[27] Aizu Y and Asakura T 2015 *Spatial filtering velocimetry: fundamentals and applications* (Berlin, Heidelberg: Springer) p. 116
[28] Schaeper M and Damaschke N 2017 *Meas. Sci. Technol.* **28** 055008
[29] Schaeper M and Damaschke N 2011 *Int. Conf. DBLP* **6752** 303
[30] Aizu Y and Asakura T 2015 *Spatial Filtering Velocimetry: Fundamentals and Applications* (Springer)
[31] Papoulis A and Hoffman J G 1967 *Phys. Today* **20** 1135
[32] Zhou J and Long X 2010 *Opt. & Laser Technol.* **42** 1038
[33] Mellmann J 2001 *Powder Technol.* **1183** 251
[34] Pohlman N A, Meier S W, Lueptow R M and Ottino J M 2006 *J. Fluid Mech.* **560** 355
[35] Jop P, Forterre Y and Pouliquen O 2005 *J. Fluid Mech.* **541** 167
[36] Alexander A, Shinbrot T and Muzzio F J 2002 *Powder Technol.* **126** 174
[37] Félix G, Falk V and D'Ortona U 2007 *Eur. Phys. J. E* **22** 25